Rapid Multi-contrast Brain Imaging on a 0.35T MR-linac

Running Title:

0.35T Quantitative Multicontrast Imaging

Siamak P. Nejad-Davarani, PhD†
Department of Radiation Oncology
Henry Ford Cancer Institute
2799 West Grand Blvd.
Detroit, MI 48202
USA
snejad1@hfhs.org

Niloufar Zakariaei, MS†
Department of Radiation Oncology
Henry Ford Cancer Institute
2799 West Grand Blvd.
Detroit, MI 48202
USA
nzakari1@hfhs.org

Yongsheng Chen, PhD
Department of Neurology
Wayne State University School of Medicine
4201 St Antoine Blvd, 8C UHC
Detroit, MI 48201
USA
ys.chen@wayne.edu

E. Mark Haacke, PhD
Department of Radiology

This article has been accepted for publication and undergone full peer review but has not been through the copyediting, typesetting, pagination and proofreading process, which may lead to differences between this version and the Version of Record. Please cite this article as doi: 10.1002/MP.14251

Wayne State University School of Medicine
Detroit, MI 48201
USA

The MRI Institute for Biomedical Research
30200 Telegraph Rd, STE 104
Bingham Farms
MI 48025
USA
nmrimaging@aol.com

Newton J Hurst, MD, PhD
Department of Radiation Oncology
Henry Ford Cancer Institute
2799 West Grand Blvd.
Detroit, MI 48202
USA
NHurst2@hfhs.org

M Salim Siddiqui, MD, PhD
Department of Radiation Oncology
Henry Ford Cancer Institute
2799 West Grand Blvd.
Detroit, MI 48202
USA
MSIDDIQ3@hfhs.org

Lonni R Schultz, PhD
Department of Public Health Sciences
Henry Ford Health System
One Ford Place, Ste 3E
Detroit, MI 48202

LSCHULT1@hfhs.org

James M Snyder, MD
Departments of Neurosurgery and Neurology
Henry Ford Health System
2799 West Grand Blvd.
Detroit, MI 48202
USA
JSNYDER5@hfhs.org

Tobias Walbert, MD
Departments of Neurosurgery and Neurology
Henry Ford Health System
2799 West Grand Blvd.
Detroit, MI 48202
USA
TWALBER1@hfhs.org

Carri Glide-Hurst, PhD, DABR*
Department of Radiation Oncology
Henry Ford Cancer Institute
2799 West Grand Blvd.
Detroit, MI 48202
USA
churst2@hfhs.org

† Authors contributed equally at first authors

* Corresponding author

ABSTRACT

Purpose: Magnetic resonance-guided radiation therapy (MRgRT) has shown great promise for localization and real-time tumor monitoring. However, to date, quantitative imaging has been limited for low field MRgRT. This work benchmarks quantitative T1, R2* and Proton Density (PD)-mapping in phantom on a 0.35T MR-linac and implements a novel acquisition method, **ST**rategically **A**cquired **G**radient **E**cho (STAGE). To further validate STAGE in a clinical setting, a pilot study was undertaken in a cohort of brain tumor patients to elucidate opportunities for longitudinal functional imaging with an MR-linac in the brain.

Methods: STAGE (two triple-echo gradient echo (GRE) acquisitions) was optimized for a 0.35T low-field MR-linac. Simulations were performed to choose two flip angles to optimize signal-to-noise ratio (SNR) and T1-mapping precision. Tradeoffs between SNR, scan time, and spatial resolution for whole-brain coverage were evaluated in healthy volunteers. Data were inputted into a STAGE processing pipeline to yield 4 qualitative images (T1-weighted, enhanced T1-weighted, proton-density (PD) weighted, and simulated FLuid-Attenuated Inversion Recovery (sFLAIR)), and 3 quantitative datasets (T1, PD, and R2*). A benchmarking ISMRM/NIST phantom consisting of vials with variable $NiCl_2$ and $MnCl_2$ concentrations was scanned using variable flip angles (VFA) (2-60 degrees) and inversion recovery (IR) methods at 0.35T. STAGE and VFA T1 values of vials were compared to IR T1 values. As measures of agreement with reference values and repeatability, relative error (RE) and coefficient of variability (CV) were calculated, respectively, for quantitative MR values within the phantom vials (spheres). To demonstrate feasibility, longitudinal STAGE data (pre-treatment, weekly, and ~2 months post-treatment) were acquired in an IRB-approved pilot study of brain tumor cases via the generation of temporal and differential quantitative MRI maps.

Results: In the phantom, RE of measured STAGE and VFA T1 relative to IR reference values were 7.0 ± 2.5% and 9.5 ± 2.2%, respectively. RE for the PD vials was 8.1%±6.8% and CV for phantom R2* measurements was 10.1% ± 9.9%. Simulations and volunteer experiments yielded final STAGE parameters of FA=$50^o/10^o$, 1x1x3 mm^3 resolution, TR=40ms, TE=5/20/34ms in 10 minutes (64 slices). In the pilot study of brain tumor patients, differential maps for R2* and T1 maps were sensitive to local tumor changes and appeared similar to 3T follow up MRI datasets.

Conclusion: Quantitative T1, R2*, and PD mapping are promising at 0.35T agreeing well with reference data. STAGE phantom data offer quantitative representations comparable to traditional methods in a fraction of the acquisition time. Initial feasibility of implementing

STAGE at 0.35T in a patient brain tumor cohort suggests that detectable changes can be observed over time. With confirmation in a larger cohort, results may be implemented to identify areas of recurrence and facilitate adaptive radiation therapy.

Keywords:

MR-Linac, Multi-contrast imaging, tumor response, quantitative MRI, low-field MRI

Introduction

The advent of MRI guided radiation therapy (MRgRT) has made real-time tumor localization and tracking possible, mainly due to the excellent soft tissue contrast and the non-ionizing nature provided by MRI[1]. By acquiring longitudinal MRI during the therapeutic treatment window, geometric variations of the tumor volume and position can be detected and tracked during the treatment course and these data can be used to facilitate adaptive radiation therapy (ART)[2]. Typically, temporal anatomical and geometrical changes of organs at risk serve as clinical indicators for ART based on proximity to the tumor, however to date, the acquisition of quantitative MR images (qMRI) using MRgRT has been limited. In the brain, qMRI has shown significant promise for defining tumor margins, assessing invasion[3], and quantifying tumor changes after treatment[4]. One such type of qMRI, R2*, has been shown to be effective for determining the grade of gliomas and distinguishing between benign and malignant tumors at 3T[5]. However, at low field strengths, the susceptibility effects become negligible as R2* approaches true R2 values[12]. Importantly, R2* values have been shown to characterize gliomas better than ADC values derived from DWI[5]. Similarly, T1 values obtained from qMRI have been shown to indicate early tumor response[6], with quantitative T1 mapping detecting enhancing tumor earlier than conventional contrast-enhanced T1-weighted images[7].

Despite the strong potential of qMRI for tumor response assessment, limited reports exist of using MRgRT to acquire qMRI data during the RT treatment course. The first study for tumor response assessment using a 0.35T MR-Co 60 RT system[8] was based on changes in ADC maps in patients with head and neck cancer, rectal cancer, and sarcoma. Furthermore, a recent multi-institutional study reported the feasibility and accuracy of performing qMRI on a 1.5T MRgRT system using a benchmarking phantom[9]. In this study, T1, T2, ADC maps, and dynamic contrast-enhanced (DCE) images were demonstrated in a patient with prostate cancer.

Recently, a novel multi-contrast multi-parametric MRI method, STrategically Acquired Gradient Echo (STAGE), was introduced using a diagnostic 3.0 T MRI that can produce several quantitative (multi-echo quantitative susceptibility (QSM), T1, PD and R2* maps) and qualitative (T1-weighted (T1W), enhanced T1-weighted (T1WE), proton-density weighted (PDW)) datasets[10-12]. The STAGE acquisition and post-processing pipeline offer distinct advantages over acquiring individual sequences by acquiring only two unique sequences that are then used to produce several qualitative images and quantitative maps, thereby not only reducing acquisition time but also co-registration uncertainties. Thus, STAGE is a practical choice for acquiring routine qMRI images during the RT course. This work demonstrates the feasibility of using STAGE on a 0.35T MR-linac, first benchmarking several quantitative sequences in a well characterized phantom, optimizing the sequence for human scanning, and then implementing STAGE in a pilot study of brain tumor patients, with the overall clinical endpoint of integrating STAGE to facilitate tumor response assessment or functional ART.

Methods

STAGE Method and Optimization

The original STAGE method consists of acquiring two dual echo scans acquired with a pair of optimal flip angles (FAs) (one smaller than the Ernst angle of white matter and the other angle larger) to produce proton density (PD) weighted and T1-weighted images[10]. For adaptation of STAGE to 0.35T, we modified the protocol to acquire images with three echoes to improve the curve fitting for estimation of the R2* maps. Phase and magnitude data were then inputted into a post-processing pipeline developed in MATLAB (The MathWorks, Inc., Natick, Massachusetts, United States). T1 and PD maps were created using the variable flip angle (VFA) method[13,14] for the two sets of images (one for each FA) at each echo and averaging the maps from each calculation. To create the enhanced T1 weighted (T1WE) image, each echo of PDW image is subtracted from the corresponding T1W images and the results are averaged. R2* maps are calculated using the three echoes for each scan and averaging the two resulting maps[10] as described in the Appendix.

To translate STAGE to low field, several optimizations were necessary. Initial FAs were determined by maximizing the sum of gray/white matter contrast (GM/WM_{CNR}) and whole brain T1 mapping precision (described as the product of dynamic range (DR) and fractional signal of points (FS))[10,14] as described in detail in Appendix. FA optimization was performed separately for both phantom and humans to ensure appropriate parameter selection to maximize precision.

Protocol optimization for humans consisted of imaging healthy volunteers and performing tradeoffs between signal to noise ratio (SNR), scan time, and spatial resolution for whole-brain coverage. At higher field strengths, radiofrequency transmit factors are taken into account for STAGE processing[23]. However, at low fields such as 0.35T for this study, the impact is expected to be less significant[2]. To further reduce the potential for slice-profile induced errors, in vivo data was acquired with 12.5% oversampling in partition direction which ensured a relative flat profile region of the brain. The final scanning parameters for phantom and *in vivo* imaging are summarized in Table 1.

Phantom Benchmarking

As qMRI on a 0.35T MR-linac has not been previously demonstrated, a National Institute of Standards and Technology (NIST) traceable ISMRM/NIST Phantom (SN: 0088)[15,16] was implemented for two purposes: (1) to compare standard qMRI sequences for T1 mapping to the phantom manufacturer stated results at 1.5T and 3T and (2) to compare the experimental STAGE to standard qMRI results at 0.35T. The ISMRM/NIST phantom consists of multiple layers with embedded vials (spheres) spanning a wide range of values for T1, T2, and proton density (via varied $NiCl_2$, $MnCl_2$ and H_2O concentrations, respectively). All phantom experiments were performed on a double-donut superconducting 70 cm diameter bore 0.35T MRI coupled with a 6 MV flattening filter free linear accelerator (MRIdian Linac (ViewRay, Mountain View, CA) using a 4-channel surface coil (Figure 1).

First, to benchmark qMRI at 0.35T, T1 mapping was performed using two well-established conventional methods: VFA[11,13,14] and inversion recovery (IR) which is considered the gold standard in T1 mapping[17]. VFA data were acquired using the parameters shown in Table 1 with FAs used in the phantom for T1 mapping were 5°, 15°, and 30° due to low SNR in lower FAs and deviations of the data from the model for higher FAs as illustrated in the Appendix (Fig A.2.a). The selection of FAs were also based on simulations with an emphasis on vials with T1 > 150 ms as this range is most similar to brain tissue. The need to correct for B_1 field variations was assessed as this has been shown to present inaccuracies at higher field strengths[11,13,14]. IR imaging was performed using a spin echo sequence with parameters shown in Table 1. Due to long scan times, IR images were acquired for a single slice, intersecting the center of the T1 mapping vials of the phantom and the IR measurement was conducted only once. 0.35T T1 mapping results were compared to values obtained at 1.5T and 3.0T as stated in the phantom manual[18]. VFA and IR data acquired at 0.35T were also used to evaluate the agreement of experimental T1 maps generated via STAGE as described in the next section.

To benchmark STAGE in phantom, PD, R2* and T1 maps at 0.35T, phantom images were acquired using FAs of 5°, 17° and 32°. To create the phantom PD maps, images acquired with FAs of 17° and 32° were used and for the R2* maps, data from all three FAs were utilized. STAGE PD maps were normalized by setting the PD value in the normal appearing white matter (NAWM) to 66 p.u. as reported by Blystad et al.[19] The estimated PD and R2* values in the phantom vials were compared with the nominal H_2O and $MnCl_2$ concentrations, respectively, within each vial as reported in the phantom manual[18]. To maximize quantification precision for a given T1, at least two FAs are required (one smaller than the Ernst angle of white matter and the other angle larger[14]). Because of a wide range of T1 values, we prioritized spheres 5 and 6 with T1 values similar to GM and WM at 0.35T (~ 650 ms and ~ 420 ms, respectively[19]). The largest selected FA for STAGE T1 quantification was 32°.

Repeatability Experiments

To investigate the repeatability of the PD, R2*, and T1 measurements, STAGE phantom imaging was conducted at 4 sessions over six weeks (sessions 1-3: 1 acquisition, session 4: 6 acquisitions), yielding a total of 9 STAGE acquisitions. Six VFA datasets were acquired in one month over separate sessions due to long scan times. Before each experiment, the phantom was allowed to thermally equilibrate in the scan room. Phantom temperature was measured before and after each imaging session with the average recorded as the phantom temperature for that acquisition.

Statistical Analysis

To quantify agreement with the stated reference values, the relative error (RE) was calculated as 100 times the absolute difference between the measured and reference values divided by the reference value. For STAGE PD, the reference data were nominal PD values of the vials. To test for agreement among T1-mapping methods at 0.35 T within each vial, the IR T1 value (n = 1) was compared to the mean for all of the VFA (n = 6) and STAGE (n = 9) measurements using one sample t-tests. Within each vial, the means for the VFA and STAGE measurements were compared to each other using two sample t-tests. Differences with a p-value less than 0.05 were considered significant with all analyses conducted using SAS version 9.4 (SAS Institute Inc., Cary, NC).

To assess repeatability, coefficient of variation (CV, or the standard deviation of all measurements for each vial, divided by their mean) was calculated for the STAGE derived PD, R2* and T1 as well as the VFA measurements. Intra-session repeatability was measured across

the 6 repeated measurements acquired at the 4th session. Inter-session repeatability was calculated across sessions 1-3 and the first measurement of the 4th session. To assess inter-session repeatability for T1 mapping using VFA, six single VFA measurements were used.

STAGE Imaging in Human Subjects

Human subjects were consented to a study approved by the Institutional Review Board. To translate STAGE to humans, acquisition parameters were optimized in a volunteer cohort imaged in the treatment position using head and neck phase array surface coils with 5 anterior and 5 posterior elements. To accommodate the immobilization, a novel 3D printed head rest was developed to fit the posterior aspect of the surface coil by first scanning the coil with an EinScan-Pro+ 3D scanner using structural light scanning methodology to capture surface data and output a stereolithography file to generate the 3D printed headrest[20]. Final fabrication was conducted using a MakerBot Replicator using a standard 3D printer filament (Acrylonitrile-Butadiene-Styrene Copolymer (ABS), 5% infill, 3 shells) and fused deposition modeling.

To establish the feasibility of applying STAGE in patients with brain tumors, four patients (1 right parietal glioblastoma (GBM) near total gross resection, 1 left parietal/occipital GBM subtotal resection, and 2 patients who were not surgical candidates (1 bifrontal oligodendroglioma and 1 GBM) undergoing MRgRT were enrolled in an IRB-approved prospective pilot study. Patients were treated to a total dose of 50.4 to 60 Gy in 2 Gy/fraction to the planning target volume. STAGE imaging was performed pre-treatment (at the time of simulation), weekly during RT, and at the two month follow up after the end of treatment. Corresponding routine diagnostic MRIs including FLuid-Attenuated Inversion Recovery (FLAIR), apparent diffusion coefficient (ADC), T2 weighted, and pre/post-Gd enhanced T1-weighted sequences were also evaluated.

Image Processing

Phantom Images

T1, R2* and PD values of each phantom vial were measured for all qMRI mapping methods by averaging the intensity of voxels of a volume within each vial. A 3D binary mask (sphere with radius of 4 voxels centered on the phantom vial to avoid partial volume effects) was applied to calculate the mean values for each vial. Because the T1 map derived from IR consisted of a single slice acquisition and 5 mm slice thickness, T1 values were measured from a single slice within a circle of radius 4 pixels.

Images of Human Subjects

To investigate intra-subject temporal variations in the serial STAGE-derived brain maps throughout the treatment course, images were rigidly co-registered to the pre-treatment STAGE T1W scan using SPM12[21] software (Statistical Parametric Mapping, Functional Imaging Laboratory, The Wellcome Trust Centre for NeuroImaging, University College London). Follow up diagnostic images acquired at 3T were also co-registered to the STAGE pre-treatment simulation T1W images. To highlight changes in the R2*, T1 and PD maps over the treatment course, differential maps were generated by performing voxelwise subtraction[7] of the registered maps[22] at different timepoints, relative to the reference image, which were the images acquired at the time of simulation.

Results

Phantom Benchmarking

Results of phantom benchmarking are shown in Figure 2. Figure 2a displays the mean PD values derived from STAGE for six repeated measurements and revealing a strong association between the measured PD values and water concentration (R^2 = 0.999). When compared to the nominal PD, the RE across all vials was 8.05% ± 6.85% (range: 1.36% - 22.90%). Figure 2b shows the measured STAGE R2* values within each vial plotted against the $MnCl_2$ concentrations (0.013-1.704 mM/L) for the T2 array, yielding a strong association (R^2 = 0.998).

Figure 2c summarizes T1 values obtained from STAGE as compared to conventional VFA and IR methods at 0.35T as well as reporting the manufacturer-stated values obtained at 1.5T and 3.0T. Since IR is considered the gold standard for T1 mapping[2], we compared VFA and STAGE derived T1 values to IR at 0.35 T. T1 values estimated by the VFA method demonstrated closer agreement to IR with the mean RE across all vials and the six VFA measurements of 7.0 ± 2.5% and the highest RE belonging to vial # 10 (10.5%). By comparison, the RE for the experimental STAGE T1 measurements with respect to the IR T1 values was 9.5 ± 2.2% (range: 5.4% - 11.2%) across all vials.

In theory, based on the Ernst angle estimation to maximize precision in T1 mapping and the largest FA that was used for T1 mapping (FA = 32°), the lowest required T1 value for quantification would be >255 ms. However, for spheres 8~11 (60 <T1<200 ms), reasonable

agreement was observed as summarized in Figure 2c. Likewise, for VFA, the lowest required T1 value for quantification is >96 ms, but we obtained reasonable accuracy for sphere 11 with T1 ~65 ms which is also highlighted in Figure 2c.

Overall, our experimental STAGE-derived T1 measurements were lower than the corresponding IR values for all vials ($p < 0.05$) as summarized in Table 2. Similarly, STAGE T1 values were lower than VFA for 7 out of 11 vials ($p < 0.05$). By comparison of two conventional techniques, the means of the VFA T1 measurements were significantly lower than the corresponding IR T1 values for all but phantom vials 3 and 4 which represent normal tissue gray matter (T1 at 1.5T = 1012 ms) and white matter (T1 at 1.5T = 730 ms), respectively.

Measurement repeatability

Table 3 summarizes the CVs as a measure of repeatability for all STAGE and VFA T1 measurements. Mean intra-session CV across the 12 PD vials (10%-90%) was 2.52 ± 1.88% (range: 0.84% (80% vial) - 7.97% (15% vial)) and the inter-session CV across all vials was 7.51% ± 5.75% (range: 2.27% (80% vial) – 20.09% (15% vial)). For R2* measurements, the intra-session CV across all vials was 8.95% ± 7.74% (range: 0.68% - 27.77%) and the inter-session CV was 10.06% ± 9.90% (range: 0.43%- 37.33%). The CV of T1 values based on the VFA measurements across all vials was 3.62% ± 0.66% (range: 2.55% - 5.29%) within all six inter-session acquisitions. The inter-session CV of T1 values across the four STAGE sessions was higher than the VFA (4.71% ± 2.35% (range: 1.83% -10.63%)). The recorded temperature across the four STAGE acquisition sessions ranged between 20.5°C and 23.0°C and for the VFA acquisitions ranged from 18.5°C to 21.4°C.

Results in Human Subjects

Our preliminary results in human subjects found that 4 qualitative maps (T1W, PDW, pT2W, sFLAIR) and 4 quantitative maps were promising for use, however QSM (SWI) did not produce useable signal due to low SNR and no natural susceptibility effects being observed at 0.35T unless a prohibitively long echo time were to be used. Sequences were optimized to have an acquisition time <10 minutes. Figure 3 shows example 0.35T STAGE images of a patient with a GBM located in the right temporal lobe after both surgery (subtotal resection) and

radiation therapy to a total dose of 60 Gy. Data includes the acquired T1W and PDW, the derived qualitative images (pT2W, T1WE) and the derived quantitative maps (PD, T1 and R2*). Residual tumor can be observed as hyper-intense regions in the T1 and PD maps, sFLAIR images, and as regions with reduced intensity in the corresponding R2* map and T1W images. Overall, clinically acceptable image quality was obtained on a 0.35T MR-linac for the following qualitative (T1W, PDW, pT2W, FLAIR and T1WE) and quantitative (T1, PD and R2*) maps.

Figure 4 shows the STAGE derived R2*, T1 and PD maps of another patient with a left occipital GBM at the time of simulation, at the end of radiation therapy (Week 7) and at the two month follow-up after the end of treatment (2 months post treatment). For comparison, corresponding diagnostic 3T images (FLAIR, Post-Gd T1W and apparent diffusion coefficient (ADC) map) acquired ~2.5 months after the end of treatment are also shown. Overall, serial qMRI changes can be observed in these maps acquired during the treatment course. In the T1 maps, prolonged T1 relaxation times can be observed at the 2 month post-treatment STAGE timepoint that correlated with progression of the enhancing tumor noted in the corresponding 3T follow up post-Gd MRI. Patterns of increased intensity in the PD maps and decreased intensity in the R2* maps for the 2 months post-treatment STAGE images appeared similar to the enhancements in the FLAIR image and ADC maps acquired in the follow up 3T datasets. The differential maps between initial and final timepoints readily highlight regions of increased T1 and PD values and reduced R2* values for the quantitative STAGE maps over the treatment course.

STAGE derived T1, R2* and PD differential maps of a post-surgical patient with a right parietal GBM are shown in Figure 5. These maps highlight differences between the first week of treatment (Start of Treatment) and two months post treatment follow-up in three axial slices. Corresponding diagnostic 3T MRI T2-FLAIR, T1 Post Gd and ADC maps acquired at 2 weeks after the end of treatment (2 Weeks Post Treatment) are also displayed for comparison purposes. STAGE T1, R2* and PD voxel-based differential maps suggest that the spatial pattern of intensity changes resemble the morphology of the lesion observed in diagnostic 3T MRI, thus suggesting that changes in the differential maps may be potentially sensitive to physiological changes within the brain

The mean T1 values within the normal-appearing white matter (NAWM) for the patients shown in Figures 4 and 6 across the three timepoints (pre-treatment, end of treatment, and follow-up) ranged from ~383 to 397 ms and yielded stable results (CV <1.5%). In contrast, the mean T1 value within the tumor volumes demonstrated much larger variations across the timepoints, with CVs of 22.4% and 10.3% for Figures 4 and 6, respectively. Relative to the mean T1 value of the tumor at baseline for Figures 4 for a left occipital glioblastoma, T1 values within the tumor volume increased by 62.4% from simulation to follow up timepoints. As shown in Figure 6 for a patient with bi-frontal oligodendroglioma, a decrease in mean T1 values of 22.3% can be observed from initial simulation to follow-up. Similarly, R2* values within the NAWM had lower variation compared to the tumor region (CV_{NAWM}/CV_{Tumor} =0.8/17.3% and CV_{NAWM}/CV_{Tumor} = 1.1/43.1% for Figures 4 and 6, respectively). The mean R2* value in the NAWM region ranged from 12.6 to 13.1 s^{-1} across the three timepoints for the two patients. By comparison, the mean values within the tumor regions for the initial simulation, end of treatment, and post-treatment timepoints were 9.0 s^{-1}, 9.6 s^{-1}, and 6.3 s^{-1} (glioblastoma, Figure 4) and 5.94 s^{-1}, 6.79 s^{-1}, 8.50 s^{-1} (oligodendroglioma, Figure 6), respectively."

In Figure 6, serial STAGE images and maps of a patient with Bi-frontal Oligodendroglioma acquired at three timepoints (At the time of RT simulation (Week 0), the last week of treatment (Week 6) and at the two month follow-up) show intensity changes within the tumor volume during the course of RT. Size reduction of the hyper-intense region in the PD and T1 maps and FLAIR images as well as the hypo-intense region in the R2* map and T1W images suggest tumor response to RT.

Discussion

This work sought to demonstrate the feasibility of using an experimental STAGE technique for qMRI on a 0.35T MR-linac including initial parameter optimization, phantom benchmarking, and implementing the technique serially in brain cancer patients to demonstrate feasibility of implementing STAGE to track changes in brain lesions during RT.

PD values measured in the ISMRM/NIST phantom by the STAGE sequence showed high correlation with the water concentration in the vials. Previously, Kumar *et. al* quantified PD

values in the same phantom on a 3T system, using a synthetic MRI sequence[23] (QRAPMASTER[24]). They obtained an RE of ~5% through repeated measures (n = 8, over the course of 2 days) while the average RE for our experimental PD measurements was of similar magnitude (~8%). Typical intracranial brain tissue PD values fall within a relative H2O content range of 50-100%[25], thus another study using the QRAPMASTER sequence at 1.5T[26] evaluated PD values of a Eurospin II (TO5) phantom (Diagnostic Sonar, Livingston, Scotland), yielding a RE of up to ~6%. For our results at 0.35T for the PD values with H2O content > 50%, the RE of was 3.13 ± 1.61%. At 1.5T, the inter-session CV of PD values measured over 11 timepoints ranged from 1.2% to 5.5%, while our results at 0.35T were of a similar magnitude (inter-session and intra-session PD CV had a range of 2.2%-8.6%. and 0.84%-1.95%, respectively).

In a manner similar to PD, the R2* values measured based on the STAGE sequence showed strong association (R^2 = 0.997) with the $MnCl_2$ concentration within the vials. In a study by Chen *et al*[27] that was also conducted at 0.35T, a strong association (R^2 = 0.998) between the $MnCl_2$ concentration and R2* values measured using ultrashort TE (UTE) sequences was also reported, although the range of the $MnCl_2$ concentration in their phantom differed from that in the ISMRM/NIST phantom (2-16 mM/L vs. 0.013-1.704 mM/L, respectively). Nevertheless, a linear relationship was observed in a similar manner to our results while the slope was slightly higher than in our results (0.07 vs 0.04 Hz/mM).

Overall, good agreement was observed between STAGE-based T1 estimations and gold standard T1 values measured by IR at 0.35T. These results are comparable to errors reported in other studies that have been conducted using the ISMRM/NIST phantom for NMR relaxation time quantifications at higher field strengths[3-6]. Jiang et al. performed a study using the ISMRM/NIST phantom to investigate the repeatability of T1 and T2 mapping using MR fingerprinting methods over 34 consecutive days[6] and showed <5% CV over all measurements. Similarly, the majority of our intra/inter-session STAGE T1 and inter-session VFA measurements at 0.35T yielded CVs <5%. Kumar et al. used the QRAPMASTER sequence at 3.0T and found that the RE of T1 measurements was 1.9%[5]. In one study across different MRI systems, T1 was assessed based on the IR and VFA methods using the same ISMRM/NIST phantom[4]. It was observed that both at 1.5T and 3T, while the IR measurements had good agreement with known T1 values, VFA measurements showed higher RE in all sites[4]. One potential reason for higher REs in VFA measurements is that the susceptibility of the estimated values to different sources of uncertainty and noise[7]. For completeness, T1 values of all vials were evaluated for STAGE, IR, and VFA at 0.35 T. However, the Ernst angle estimation

suggests that precision would be maximized at a subset of these data due to the FAs implemented in the analysis (i.e., STAGE T1 > 255 ms and VFA T1 > 96 ms). Nevertheless, reasonable accuracy was observed across all vials evaluated, suggesting overall robustness in our methods.

Over the course of phantom measurements, temperature variations were <3°C. Compared to other ions, using Nickel such as the $NiCl_2$ used in the T1 array vials of the ISMRM/NIST phantom leads to lower temperature dependence of T1[30]. T1 measurements done on a NiCl2 gel phantom showed small changes of T1 due to temperature change, especially for vials with lower T1 values, and correction was recommended only for temperature changes > 5°[31], thus no temperature corrections were performed in this work. The dependency of PD on temperature has previously been measured to be ~0.3%/°C for ex-vivo porcine tissue on a 0.5T field[32] and measurements of T2* values at 1.5T showed linear dependency of 1.5%/°C in vials with various concentrations of MnCl2[33].

For *in vivo* brain tissue, one study showed R2* values of ~15 1/s and ~21 1/s in the GM and WM regions, respectively, of healthy brain tissue at 3T[34]. Based on an empirical equation by Pohmann et al[13], the expected NAWM R2* value at 0.35T is 11.7 s^{-1} which is similar to the values observed in the normal tissue on the MR-linac (~13.0 s^{-1}). While to the best of our knowledge, measurements of R2* in cerebral tumors at 0.35T have not been reported in the literature, a study Liu et al[14] conducted at 3T reported R2* values for cerebral tumors of differing pathologies ranging from 5.20 s^{-1} to 36.95 s^{-1} as compared to the R2* of NAWM (~21 s^{-1})[15] at this field strength. The R2* values measured in the tumor region of the two patients in Figures 4 and 6 had mean values lower than the measured R2* value of the NAWM. In a previous study at 0.35T by Kjos et al[16], the mean T1 value of the normal subcortical WM was measured to be 419 ms which is of a similar magnitude of T1 in the NAWM of patients observed in this work (~383 to 397 ms). Other qMRI studies at various field strengths (0.28T[17], 0.35T[18], 0.7T[18], and 3.0T[19]) have reported increased T1 values within the cerebral tumors which is consistent with our findings based on STAGE derived T1 maps. Furthermore, given the noted changes in T1, R2*, and PD observed in the tumor volumes over the treatment course with respect to the stable values reported within the NAWM and phantom studies, STAGE-derived metrics hold promise for quantitative response assessment and will be reported along with clinical outcomes at the completion of a currently enrolling prospective clinical trial.

Aside from diffusion weighted imaging[8], our work is the first to evaluate the performance of a 0.35T MRgRT system for qMRI and introduce the potential of using STAGE based multi-

parametric qMRI maps on the MR-linac for temporal treatment response measurements in the brain. Performing this work on an MR-linac offers advantages of acquiring data throughout radiation therapy with patients immobilized in the treatment position. Our STAGE T1, R2* and PD maps of patients with brain tumors acquired during the treatment course enhanced with derived differential maps across timepoints, thus offering great potential for detecting changes in the brain tissue that may indicate treatment response, areas of necrosis, acute neuroanatomic changes, or early signs of disease progression. As shown in the differential maps generated by two GBM patients in Figures 4 and 5, T1-prolongation, decreased R2*, and increased PD values were observed in the treated volumes. T1-prolongation often indicates an increase of water content in tissue (edema)[36] with T1 mapping being more sensitive in detecting tissue changes than conventional qualitative MR images such as post-Gd MRI[37] (note STAGE T1 map enhancement in Figure 4 as compared to the corresponding post-Gd MRI). Increased PD map values may indicate the presence of edema[38] and quantitative PD has been shown to detect peritumoral edema of gliomas in regions that do not show Gd enhancement[37] which can also be observed in the STAGE PD maps in Figure 4. R2* values may indicate the oxygenation state of tumors[39] where increase of deoxygenated hemoglobin leads to increase of the R2* value (or in other words, decrease of the T2* value)[40], suggesting that if confirmed in a larger cohort, serial changes may correlate to tumor oxygenation. These data may be used to more precisely determine time points of progression during RT, which will require a detailed quantitative analysis of the serial STAGE maps in a larger cohort of patients with brain tumors.

In a recent multi-site study, qMRI images (T1, T2, ADC maps and Dynamic Contrast Enhanced (DCE) images) were acquired on a 1.5T MR-linac and demonstrated in a prostate cancer patient[9]. Similar to our work on a 0.35T MR-linac, repeated measurements on the 1.5T MR-linac also showed low inter-session CV for the T1, T2 and ADC values that were measured in phantom inserts.

A source of uncertainty in all diagnostic MRI and MRgRT systems are the distortions arising from the magnet itself (such as gradient non-linearity (GNL)) or from object/patient-induced distortions. We have previously shown on our 0.35T MR-linac that within a 10 cm radius of the magnet iso-center, GNL distortions are < 1mm[8,9]. At low fields such as the 0.35T MR-linac and a 1.0T MR-SIM, the magnitude of patient-specific susceptibility induced distortions at these field strengths were < 0.5 mm[10,11], even in the presence of large rectal air pockets. Therefore, considering the size of both the phantom (200 mm inner diameter) and the human head, the impact of GNL and susceptibility-induced distortions may be considered negligible in

this work. Extensions to disease sites further away from magnet isocenter may present additional uncertainties requiring appropriate quality assurance procedures. Low SNR has been a major concern in low field imaging given a linear dependence of the SNR as a function of the magnetic field strength[21]. Conducting STAGE measurements at 0.35 T was optimized by applying a parallel imaging acceleration factor of 2 to yield results in <10 min. Here, the first and second echoes were used for T1 mapping and then averaged to increase the SNR of the quantitative maps. With further efforts to improve the acquisition strategy and reconstruction, one can perform more than two scans in the same scanning time, which increases the SNR of quantitative maps by using more data points in the fitting. For instance, applying compressed sensing via a multi-channel blind deconvolution (MalBEC) approach has demonstrated the feasibility of achieving an acceleration factor of 4 for in-vivo brain imaging [22]. Another limitation is that the STAGE sequence parameters were optimized for imaging the gray and white matter in the brain and not for the CSF. For tissues with long T1 (e.g., CSF) the FA should be as small as possible which was not the case for our acquisition parameters, therefore the qMRI values that are estimated for the CSF are not considered reliable. Consequently, the enhanced ventricular and subdural regions in the difference maps in Figures 4 and 5 do not reflect realistic changes in the qMRI values in these regions.

As serial STAGE qMRI maps may be used to track changes in the tumor volumes during the treatment course, it is important to make assessments of systematic variations of the measured qMRI values at 0.35T to isolate variations due to physiological changes of tumors. Our results in the benchmarking phantom suggest that T1 and PD are the most robust (intra-session CV ~2-3%, inter-session CV ~5-7%) whereas R2* showed higher variability. Future work will include evaluating serial *in vivo* CV measurements of healthy brain tissue in a larger cohort to further characterize the variability. These data may then be used to identify thresholds that may indicate significant changes of qMRI data due to treatment response or disease and find clinically meaningful correlates with follow up imaging and clinical outcomes.

Conclusions

Quantitative T1, R2*, and PD mapping are promising on a 0.35T MR-linac and agree well with reference data. STAGE phantom data offer close approximations of traditional quantitative methods in a fraction of the acquisition time. Initial feasibility of implementing STAGE at 0.35T in a patient cohort suggests that detectable changes can be observed over time. With confirmation in a larger cohort, results may be implemented to identify areas of local tumor

progression and use this information to further personalize radiation therapy during the treatment course.

Acknowledgements

Research reported in this publication was supported in part by the National Cancer Institute of the National Institutes of Health under award number: R01CA204189 (Carri Glide-Hurst). The content is solely the responsibility of the authors and does not necessarily represent the official views of the National Institutes of Health. This work was also partially funded by internal grants from Henry Ford Health System (Carri Glide-Hurst) as well as the generous support of ASTRO-AAPM Physics Resident/Post-Doctoral Fellow Seed Grant (Siamak Nejad-Davarani).

Conflict of Interest

The submitting institution has research agreements with ViewRay, Inc. but no financial support was received for the current work. Carri Glide-Hurst discloses travel and honorarium from ViewRay, Inc. for speaking engagements and research agreements with Philips Healthcare.

References

1. Fischer-Valuck, B.W*., et al.* Two-and-a-half-year clinical experience with the world's first magnetic resonance image guided radiation therapy system. *Adv Radiat Oncol* **2**, 485-493 (2017).
2. Bhatnagar, P., Subesinghe, M., Patel, C., Prestwich, R. & Scarsbrook, A.F. Functional imaging for radiation treatment planning, response assessment, and adaptive therapy in head and neck cancer. *Radiographics* **33**, 1909-1929 (2013).
3. Price, S.J. & Gillard, J.H. Imaging biomarkers of brain tumour margin and tumour invasion. *Br J Radiol* **84 Spec No 2**, S159-167 (2011).
4. Deng, J. & Wang, Y. Quantitative magnetic resonance imaging biomarkers in oncological clinical trials: Current techniques and standardization challenges. *Chronic Dis Transl Med* **3**, 8-20 (2017).
5. Liu, Z., Liao, H., Yin, J. & Li, Y. Using R2* values to evaluate brain tumours on magnetic resonance imaging: preliminary results. *Eur Radiol* **24**, 693-702 (2014).
6. McSheehy, P.M*., et al.* Quantified tumor t1 is a generic early-response imaging biomarker for chemotherapy reflecting cell viability. *Clin Cancer Res* **16**, 212-225 (2010).

7. Lescher, S.*, et al.* Quantitative T1 and T2 mapping in recurrent glioblastomas under bevacizumab: earlier detection of tumor progression compared to conventional MRI. *Neuroradiology* **57**, 11-20 (2015).
8. Yang, Y.*, et al.* Longitudinal diffusion MRI for treatment response assessment: Preliminary experience using an MRI-guided tri-cobalt 60 radiotherapy system. *Med Phys* **43**, 1369-1373 (2016).
9. Kooreman, E.S.*, et al.* Feasibility and accuracy of quantitative imaging on a 1.5 T MR-linear accelerator. *Radiotherapy and Oncology* **133**, 156-162 (2019).
10. Chen, Y., Liu, S., Wang, Y., Kang, Y. & Haacke, E.M. STrategically Acquired Gradient Echo (STAGE) imaging, part I: Creating enhanced T1 contrast and standardized susceptibility weighted imaging and quantitative susceptibility mapping. *Magn Reson Imaging* **46**, 130-139 (2018).
11. Wang, Y.*, et al.* STrategically Acquired Gradient Echo (STAGE) imaging, part II: Correcting for RF inhomogeneities in estimating T1 and proton density. *Magn Reson Imaging* **46**, 140-150 (2018).
12. Haacke, E.M.*, et al.* STrategically Acquired Gradient Echo (STAGE) imaging, part III: Technical advances and clinical applications of a rapid multi-contrast multi-parametric brain imaging method. *Magn Reson Imaging* **65**, 15-26 (2019).
13. Venkatesan, R., Lin, W. & Haacke, E.M. Accurate determination of spin-density and T1 in the presence of RF-field inhomogeneities and flip-angle miscalibration. *Magn Reson Med* **40**, 592-602 (1998).
14. Deoni, S.C., Rutt, B.K. & Peters, T.M. Rapid combined T1 and T2 mapping using gradient recalled acquisition in the steady state. *Magn Reson Med* **49**, 515-526 (2003).
15. Russek, S.E.*, et al.* Characterization of NIST/ISMRM MRI System Phantom. in *ISMRM 20th Annual Meeting and Exhibition, 5-11 May, 2012, Melbourne, Australia*.
16. Jiang, Y.*, et al.* Repeatability of magnetic resonance fingerprinting T1 and T2 estimates assessed using the ISMRM/NIST MRI system phantom. *Magn Reson Med* **78**, 1452-1457 (2017).
17. Stikov, N.*, et al.* On the accuracy of T1 mapping: searching for common ground. *Magn Reson Med* **73**, 514-522 (2015).
18. System Standard Model 130, Product Manual. (ed. QalibreMD) (Boulder, CO, 2016).
19. Kjos, B.O.*, et al.* Reproducibility of relaxation times and spin density calculated from routine MR imaging sequences: clinical study of the CNS. *AJR Am J Roentgenol* **144**, 1165-1170 (1985).

20. Glide-Hurst, C.*, et al.* Development of 3D Printed Immobilization for the MR-Linac: Toward High Precision Brain Treatments. in *MEDICAL PHYSICS*, Vol. 45 E481-E482 (WILEY 111 RIVER ST, HOBOKEN 07030-5774, NJ USA, 2018).
21. Ashburner, J. SPM: a history. *Neuroimage* **62**, 791-800 (2012).
22. Ellingson, B.M.*, et al.* Quantification of edema reduction using differential quantitative T2 (DQT2) relaxometry mapping in recurrent glioblastoma treated with bevacizumab. *J Neuro-Oncol* **106**, 111-119 (2012).
23. Kumar, N.M.*, et al.* Synthetic MRI of the Knee: Phantom Validation and Comparison with Conventional MRI. *Radiology* **289**, 465-477 (2018).
24. Warntjes, J.B., Dahlqvist, O. & Lundberg, P. Novel method for rapid, simultaneous T1, T2*, and proton density quantification. *Magn Reson Med* **57**, 528-537 (2007).
25. Maekawa, T.*, et al.* Effect of Gadolinium on the Estimation of Myelin and Brain Tissue Volumes Based on Quantitative Synthetic MRI. *American Journal of Neuroradiology* **40**, 231-237 (2019).
26. Krauss, W., Gunnarsson, M., Andersson, T. & Thunberg, P. Accuracy and reproducibility of a quantitative magnetic resonance imaging method for concurrent measurements of tissue relaxation times and proton density. *Magnetic Resonance Imaging* **33**, 584-591 (2015).
27. Chen, X. & Qiu, B. A pilot study of short T2* measurements with ultrashort echo time imaging at 0.35 T. *Biomed Eng Online* **17**, 70 (2018).
28. Keenan, K.E.*, et al.* NIST/ISMRM MRI system phantom T1 measurements on multiple MRI systems. in *21st Annual Meeting of ISMRM, Salt Lake City, Utah, USA, 2013* 4338.
29. Lee, Y., Callaghan, M.F. & Nagy, Z. Analysis of the Precision of Variable Flip Angle T(1) Mapping with Emphasis on the Noise Propagated from RF Transmit Field Maps. *Frontiers in neuroscience* **11**, 106-106 (2017).
30. Kraft, K.A., Fatouros, P.P., Clarke, G.D. & Kishore, P.R. An MRI phantom material for quantitative relaxometry. *Magn Reson Med* **5**, 555-562 (1987).
31. Vassiliou, V.S.*, et al.* Magnetic resonance imaging phantoms for quality-control of myocardial T1 and ECV mapping: specific formulation, long-term stability and variation with heart rate and temperature. *J Cardiovasc Magn Reson* **18**, 62 (2016).
32. Chen, J., Daniel, B.L. & Pauly, K.B. Investigation of proton density for measuring tissue temperature. *J Magn Reson Imaging* **23**, 430-434 (2006).

33. Smith, G., Carpenter, J.-P., Mohiaddin, R., Pennell, D. & Firmin, D. A phantom study of temperature-dependent MRI T2* measurement. *Journal of Cardiovascular Magnetic Resonance* **11**(2009).
34. Weiskopf, N.*, et al.* Quantitative multi-parameter mapping of R1, PD*, MT, and R2* at 3T: a multi-center validation. *Frontiers in Neuroscience* **7**(2013).
35. Liu, Z., Liao, H., Yin, J. & Li, Y. Using R2* values to evaluate brain tumours on magnetic resonance imaging: Preliminary results. *European Radiology* **24**, 693-702 (2014).
36. Bastin, M.E., Sinha, S., Whittle, I.R. & Wardlaw, J.M. Measurements of water diffusion and T1 values in peritumoural oedematous brain. *Neuroreport* **13**, 1335-1340 (2002).
37. Blystad, I.*, et al.* Quantitative MRI for analysis of peritumoral edema in malignant gliomas. *PLoS One* **12**, e0177135 (2017).
38. Tofts, P. *Quantitative MRI of the brain : measuring changes caused by disease*, (Wiley, Chichester, West Sussex ; Hoboken, NJ, 2003).
39. Losert, C., Peller, M., Schneider, P. & Reiser, M. Oxygen-enhanced MRI of the brain. *Magn Reson Med* **48**, 271-277 (2002).
40. Liu, Z.H., Liao, H.B., Yin, J.H. & Li, Y.F. Using R2(star) values to evaluate brain tumours on magnetic resonance imaging: Preliminary results. *European Radiology* **24**, 693-702 (2014).
41. Chen, X. & Qiu, B. A pilot study of short T2* measurements with ultrashort echo time imaging at 0.35 T. *BioMedical Engineering OnLine* **17**, 70 (2018).

FIGURE CAPTIONS

Figure 1. (a) Imaging setup in the flexible 4-channel surface head coil for the ISMRM/NIST phantom scanned on a 0.35T MR-linac. (b) Example axial image of the Proton Density (PD) vials of the ISMRM/NIST phantom. (c) Example simulation implemented to select optimal flip angles (FAs) for the STAGE acquisition in the phantom for the 5th vial.

Figure 2. Measured (a) Proton Density (PD) and (b) R2* values within the phantom vials, exhibiting excellent correlation with nominal concentrations of water and MnCl2, respectively. (c) T1 values measured in 11 vials of the ISMRM/NIST phantom at 0.35T based on three different T1 mapping methods (STrategically Acquired Gradient Echo (STAGE), Variable Flip Angle (VFA), and Inversion Recovery (IR)) and the nominal manufacturer-reported T1 values for 1.5T and 3.0 T.

Figure 3. STrategically Acquired Gradient Echo (STAGE) images acquired on a 0.35T MR-linac of a patient with Glioblastoma in the right temporal lobe acquired after surgery. Data include the native T1-weighted (T1W) and proton density weighted (PDW) datasets, derived qualitative images (pseudo-T2 Weighted, T1W enhanced, and simulated FLuid-Attenuated Inversion Recovery (sFLAIR)) and quantitative maps (R2*, T1, and Proton Density (PD)).

Figure 4 T1, R2* and Proton Density (PD) maps of a patient with left occipital Glioblastoma acquired at the time of simulation, end of treatment, and 2 months post-treatment along with differential maps (subtraction of STrategically Acquired Gradient Echo (STAGE) maps acquired 2 months post-treatment from maps acquired at the time of simulation) highlighting areas of treatment response. Corresponding patterns of abnormal regions in the 3.0T diagnostic T1 post-Gd, FLuid-Attenuated Inversion Recovery (FLAIR), and Apparent Diffusion Coefficient (ADC) images acquired at the time of follow-up (2 Months Post Treatment match intensity changes in STAGE images. Histograms show intensity distribution of T1, R2* and PD maps within the (top row) normal appearing white matter (NAWM) and (bottom row) tumor region at

the three timepoints. Histograms highlight stability of map intensities within the NAWM, while the mean T1 and PD values are increased and mean R2* values are decreased at 2 months post treatment, within the tumor region.

Figure 5. (Left) Three axial slices of STrategically Acquired Gradient Echo (STAGE) derived T1, R2*, and proton density (PD) differential maps of a patient with Glioblastoma acquired at 0.35T. Differential maps were created by performing a voxel-by-voxel based subtraction of the STAGE maps acquired at 2 months follow up from corresponding maps acquired at the start of treatment. (Right) Diagnostic 3T MRI acquired 2 weeks after the end of radiation therapy (2 Weeks Post Treatment) including a T2- FLuid-Attenuated Inversion Recovery (T2-FLAIR), T1-post Gadolinium contrast, and Apparent Diffusion Coefficient (ADC) maps. The STAGE differential maps highlight brain regions with changes in quantitative MRI values at the 2 month follow up relative to maps acquired at the first fraction indicating the potential utility of STAGE for treatment response assessment. Red, Green and Yellow arrows highlight similar patterns among the lesion between the STAGE quantitative MRI maps and diagnostic images.

Figure 6. Serial STrategically Acquired Gradient Echo (STAGE) images of a patient with a Bi-frontal Oligodendroglioma acquired at the time of RT simulation (Simulation), the last week of treatment (End of Treatment), and at the two month follow-up after end of treatment (2 Months Post Treatment), showing tumor reductions over the treatment course. An outline of the tumor volume is highlighted in red on the Simulation images. Histograms of the T1, R2* and PD maps of the normal appearing white matter (NAWM) were stable across the three timepoints. In contrast, between the simulation and 2 Months Post Treatment, the mean T1 and PD for the tumor region reduced while the mean R2* increased, possibly indicating the resolution of the tumor volume as observed in the maps above.

Figure A.1. 2D Contour plots of the (a) $\mathrm{CNR}_{\mathrm{sub}}$, (b) DR×FS and (c) the sum of a and b . Each of the contours were plotted as a function of θ_1 and θ_2 to find the pair of FAs to maximize the GM/WM contrast and T1 precision. Optimal FAs for producing the best maps were determined to be θ_1 =10° for the PD map and θ_2 =50° for the T1 map.

Figure A.2. (a) Normalized spoiled gradient echo signal as a function of flip angle (FA) based on equation (A.1) and signal from the scanner acquired from the 5th vial of the T1 array with T1= 527ms. For FAs larger than 40°, the signal is not fit to the theoretical model, which leads to

exclusion of large FA (>40°) for the choice of optimal FAs. (b) Plot of equation (A.5) in the $(x(\theta), y(\theta))$ coordinates. Although in (a) error bars seem to have the same value, transformation to the mentioned plane shows that the noise effect for very small FA is higher, which leads to exclusion of small FAs ($\leq 4°$). (c) 2D contour plot for selecting of the optimal pair of FAs for the 5th vial

Table 1. MR acquisition parameters for imaging the phantom using Strategically Acquired Gradient Echo (STAGE), Variable Flip Angle (VFA) and Inversion Recovery (IR), as well as the human STAGE studies.

	TR (ms)	TE (ms)	TI (ms)	FA (°)	Field of view (mm^3)	Voxel Size (mm^3)	Scan Time (minute:second)
STAGE (Phantom)	40	5, 20.63, 34.14	0	5, 17, 32	232 X 256 X 320	1 X 1 X 5	Per scan: 4:39 Total: 12:58
STAGE (Human)	40	5, 20.63, 34.14	0	10, 50	232.5 X 310 X 192	1 X 1 X 3	Per scan: 4:39 Total: 9:18
VFA (Phantom)	15	5.35	0	5, 15, 30	256 X 256 X 240	1 X 1 X 3	Per scan: 2:33 Total: 7:09
IR (Spin Echo Sequence) (Phantom)	5000	10	0, 25, 50, 70, 100, 150, 200, 300, 500, 800,1000, 1500,2000, 2500	90	250 X 250 (mm^2)	0.97 X 0.97 (mm^2)	Per scan: 21:20 Total ~ 5hr

Abbreviations: TR = repetition time, ms = millisecond, TE = echo time, TI = inversion time, FA = flip angle, mm = millimeter

Table 2: Mean and standard deviation of the resultant T1 values for the 11 phantom vials, estimated based on inversion recovery (IR), variable flip angle (VFA), and Strategically Acquired Gradient Echo (STAGE) methods on a 0.35 T MR-linac. The last three columns indicate significance of differences for T1 values of each vial using one sample (IR vs. VFA and IR vs. STAGE) and two sample (VFA vs. STAGE) t-tests.

	IR (ms)	**VFA (ms)**		**STAGE (ms)**		***p-value***		
	(n = 1)	**(n = 6)**		**(n = 9)**				
Phantom Vial		**Mean**	**Std**	**Mean**	**Std**	**VFA vs IR[1]**	**STAGE vs IR[1]**	**VFA vs STAGE[2]**
1	2156.89	1998.65	105.73	1873.26	101.35	0.014*	<0.001*	0.029*
2	1521.58	1466.33	52.13	1325.2	69.47	0.048*	<0.001*	<0.001*
3	1025.39	1058.12	40.73	930.96	46.79	0.106	<0.001*	<0.001*
4	766.15	751.76	29.32	658.33	27.68	0.283	<0.001*	<0.001*
5	531.6	509.15	15.88	474.66	13.79	0.018*	<0.001*	<0.001*
6	388.72	353.49	9.00	346.23	8.03	<0.001*	<0.001*	0.108
7	273.54	252.05	8.2	239.84	10.03	0.001*	<0.001*	0.022*
8	200.36	185.9	7.39	172.12	6.35	0.004*	<0.001*	0.001*
9	139.99	126.86	4.57	122.76	4.52	<0.001*	<0.001*	0.094
10	97.53	87.25	2.94	85.55	4.76	<0.001*	<0.001*	0.442
11	68.99	62.38	2.09	64.71	5.39	<0.001*	0.025*	0.330

[1]p-value from one sample t-test

[2]p-value from two sample t-test

* indicates significance at the 0.05 level

Table 3. Coefficient of Variation (CV) values within the Proton Density (PD), R2, and T1 vials of the ISMRM/NIST phantom for the STAGE inter-session (n = 4) and intra-session (n = 6) values and Variable Flip Angle (VFA) T1 inter-session values (n = 6). CV values are expressed in %.*

PD Vial	**STAGE PD CV**		**T2 Vial**	**STAGE R2* CV**		**T1 Vial**	**STAGE T1 CV**		**VFA T1 CV**
H_2O (%)	**Intra-session**	**Inter-session**	**$MnCl_2$ (mM)**	**Intra-session**	**Inter-session**	**$NiCl_2$ (nM)**	**Intra-session**	**Inter-session**	**Inter-session**
N/A			**0.013**	15.93	3.63	**0.299**	2.34	5.68	5.29
10	3.27	17.31	**0.021**	27.77	22.55	**0.623**	1.61	4.54	3.56
15	7.98	20.09	**0.031**	10.95	16.86	**1.072**	1.28	2.71	3.85
20	1.28	6.06	**0.047**	18.35	13.53	**1.720**	1.68	2.34	3.90
25	3.83	12.69	**0.069**	16.02	37.33	**2.617**	1.72	1.83	3.12
30	2.88	5.43	**0.101**	10.14	12.92	**3.912**	1.67	3.17	2.55
35	2.17	2.39	**0.145**	7.53	12.46	**5.731**	0.97	5.65	3.25
40	2.58	3.66	**0.207**	5.70	4.25	**8.297**	2.44	4.58	3.98
50	1.96	4.19	**0.296**	1.71	5.80	**11.936**	2.71	4.12	3.60
60	1.29	8.63	**0.421**	2.83	2.44	**17.070**	2.95	6.56	3.37
70	1.16	3.82	**0.599**	2.65	2.51	**24.326**	6.22	10.63	3.35
80	0.84	2.27	**0.849**	0.68	0.43	**N/A**			
90	1.03	3.59	**1.104**	3.04	2.86	**N/A**			
N/A			**1.704**	2.05	3.19	**N/A**			
Mean	**2.52**	**7.51**		**8.95**	**10.05**		**2.33**	**4.71**	**3.62**
StDev	**1.88**	**5.75**		**7.74**	**9.90**		**1.36**	**2.35**	**0.66**

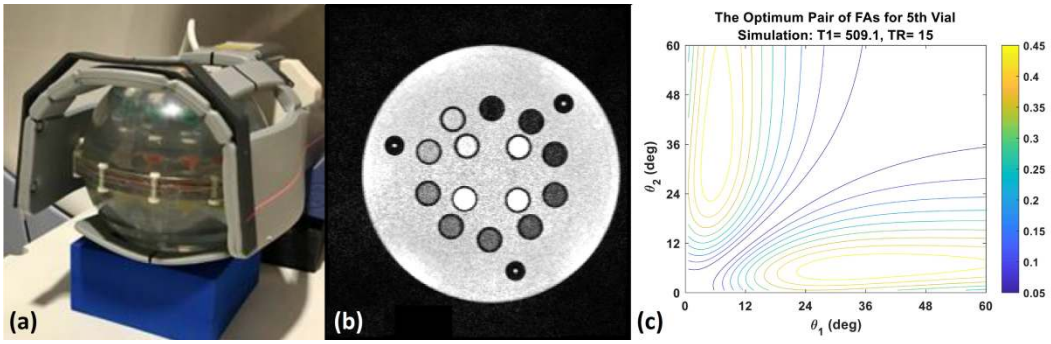

mp_14251_f1.tif

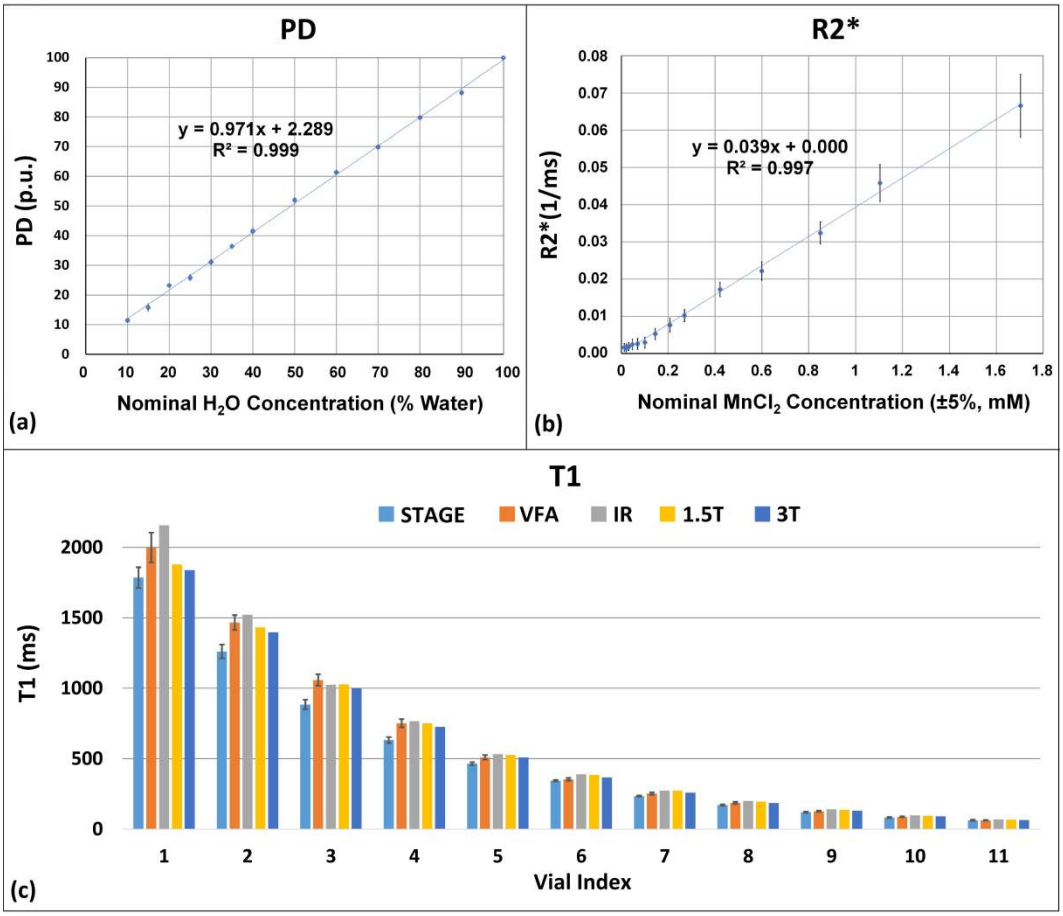

mp_14251_f2.tif

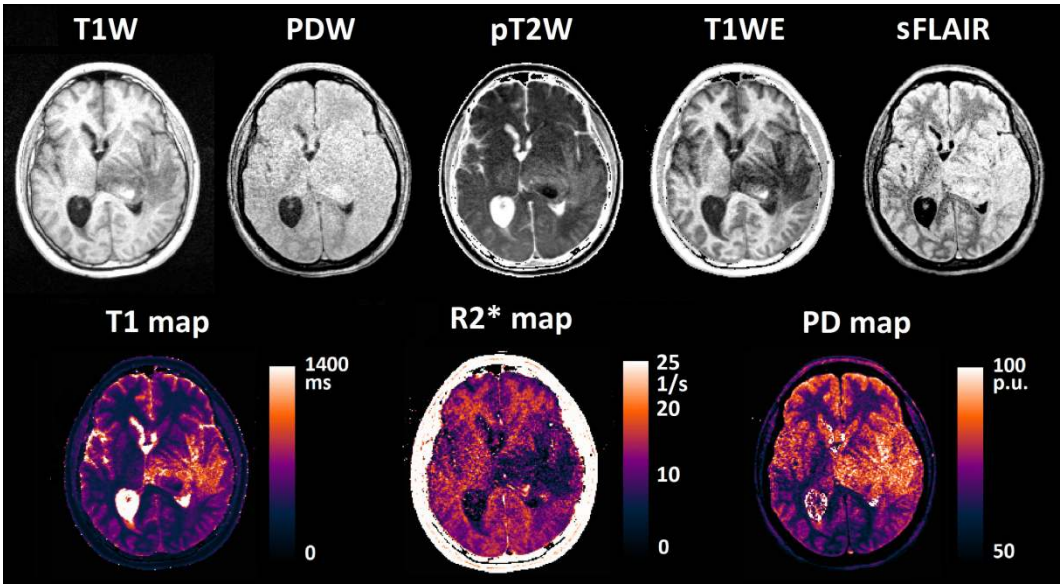

mp_14251_f3.tif

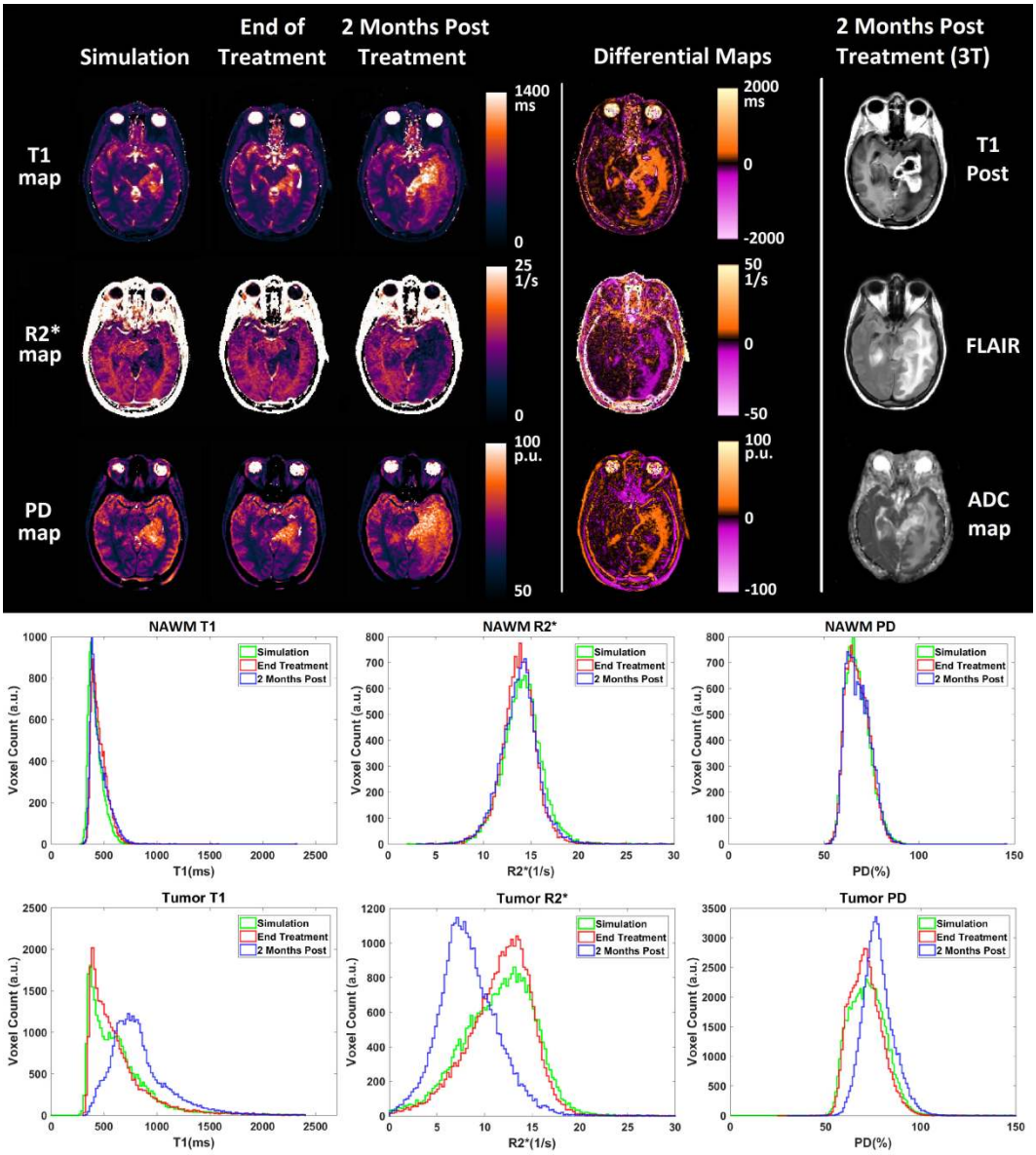

mp_14251_f4.tif

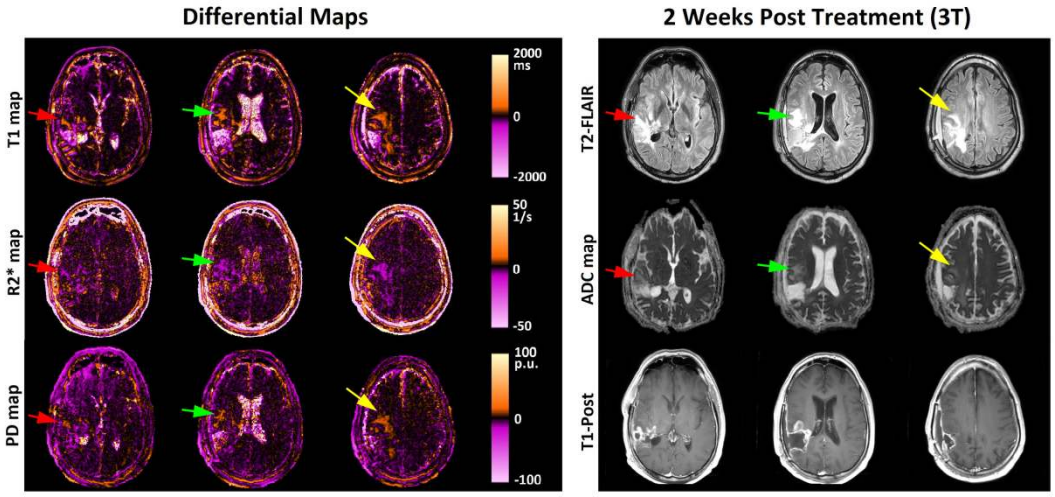

mp_14251_f5.tif

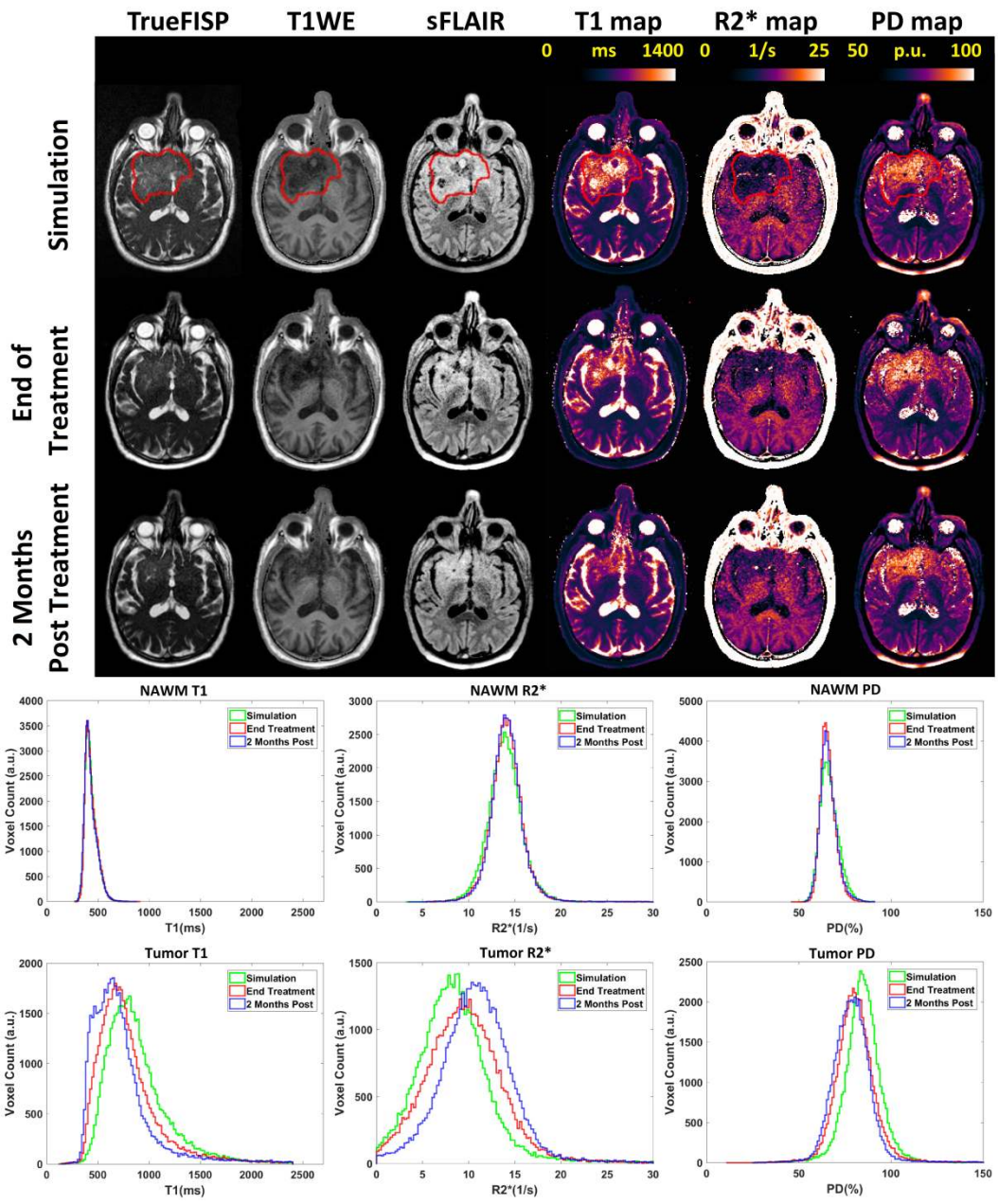

mp_14251_f6.tif